

Available online at www.synsint.com

Synthesis and Sintering

ISSN 2564-0186 (Print), ISSN 2564-0194 (Online)



Research article

A TEM study of nanostructures and interfaces in the hot-press sintered ZrB_2 -SiC-Si₃N₄ composites



Vladimir Bazhin ^a, Aleksander Nikolaev ^b, Valeria Esthefania Quiros Cabascango ^c, Changjin Shao ^d, Genrih Davletov ^b, Tatyana Gizatullina ^b, Vadim Fetisov ^{b,*}

^a Department of Metallurgy, Empress Catherine II Saint Petersburg Mining University, Saint Petersburg, Russia

^b Department of Petroleum Engineering, Empress Catherine II Saint Petersburg Mining University, Saint Petersburg, Russia

^c Independent Researcher, Quito, Ecuador

^d Department of Petroleum Engineering, China University of Petroleum-Beijing 18, Fuxue Road, Changping District, Beijing 102249, China

ABSTRACT

A fully dense ZrB_2 -30 vol% SiC composite containing 5 wt% Si₃N₄ and 4 wt% phenolic resin (1.6 wt% carbon) was sintered using the hot-pressing route under the external pressure of 10 MPa at 1900 °C for 2 h. The microstructural evolution and interfacial phenomena were scrutinized using advanced microscopy facilities such as high-resolution transmission electron microscopy (HRTEM) and field emission scanning electron microscopy (FESEM). The FESEM images showed the ZrB_2 and SiC grains without any evidence of Si₃N₄. The formation of the hexagonal BN (hBN) phase was proven in the sintered composite. The hBN nanosheets had a graphite-like morphology with an average thickness of 20 nm. This phase has a perpendicular orientation to the pressure direction and prevents abnormal ZrB_2 grain growth. Two types of ZrB_2 /SiC interfaces were detected, which exhibited an amorphous phase along with the grain boundary and a clean/smooth interface, resulting from the Si₃N₄ addition. HRTEM and inverse fast Fourier transform (IFFT) observations disclosed that the d-spacing value in the ZrB_2 grain (0.335 nm) is higher than those reported in the literature. Furthermore, it was found that the exerted pressure during the sintering distorted atomic planes. The presence of numerous dislocations within the ZrB_2 grains confirmed dislocation creep as the main densification mechanism.

© 2023 The Authors. Published by Synsint Research Group.

KEYWORDS

ZrB_2 -SiC ceramics
Si₃N₄ additive
Hot-pressing
Interface
Microstructure
Dislocation



1. Introduction

Non-oxide ceramics including nitride, carbide, and boride compounds of a few transition metal elements are categorized as ultra-high temperature ceramics (UHTCs). Based on their significant combination of characteristics such as high strength, high hardness, acceptable thermal shock resistance, high melting point, and machinability, these ceramics attracted a considerable amount of attention in applications like aerospace vehicles, propulsion systems, and in

general, high-temperature industries [1–5]. Among the UHTCs, ZrB_2 -based ceramics are in priority and are the best candidates for applications like thermal protection systems (TPS) or refractory crucibles [6]. Despite favorable features of ZrB_2 -based materials, some deficiencies, such as low sinterability because of covalent strong bonds, relatively low fracture toughness, and poor oxidation resistance, restrict the ZrB_2 -based ceramics utilization in many industries [7]. The solution to improve the properties, as mentioned above, is the addition of a secondary phase. Many studies have been carried out on the effect of

* Corresponding author. E-mail address: fetisov_v@pers.spmi.ru (V. Fetisov)

Received 7 July 2023; Received in revised form 27 December 2023; Accepted 29 December 2023.

Peer review under responsibility of Synsint Research Group. This is an open access article under the CC BY license (<https://creativecommons.org/licenses/by/4.0/>).
<https://doi.org/10.53063/synsint.2023.34165>

various reinforcements like zirconium carbide (ZrC), silicon carbide (SiC), and other materials to reduce the sintering temperature and improve the densification behavior [8, 9].

SiC additive has shown a remarkable improvement in mechanical properties, densification behavior, and sinterability than other secondary phases to the ZrB₂-based composites. As this category of UHTCs attracted lots of attention, many researchers studied different fabrication methods to achieve the highest density and most favorable properties. The main fabrication methods are hot pressing (HP) [10], spark plasma sintering (SPS) [11], and pressureless sintering (PS) [12]. However, HP and SPS are those that can lead to fully dense composites because of the applied pressure; nevertheless, sintering via the PS technique can result in components with complex geometries. However, achieving this goal by PS requires machining, which takes more time and increases the final cost of the components. Therefore, HP is considered the most favorable method to sinter ZrB₂-SiC ceramics [16–18]. Besides selecting the most suitable sintering method, using sintering additives can also be beneficial in improving the densification behavior by activation of various densification mechanisms. Considering the ZrB₂-SiC system, the most studied additives in the literature are carbides (ZrC [16], B₄C [17], and WC [18]), nitrides (ZrN [19], and HfN [20]), disilicides (MoSi₂ [21], TaSi₂ [22], and ZrSi₂ [23]), oxides (ZrO₂ [24] and Y₂O₃ [25]), carbon black [26], carbon fiber [27], etc.

Many investigations have been done on nitride additives' effect on mechanical and microstructural properties and densification behavior. The introduction of ZrN to the ZrB₂-SiC composites caused the in-situ formation of hBN flakes that increased the porosity level and lowered the Vickers hardness compared to the ZrB₂-SiC UHTCs; however, owing to the homogeneous distribution of hBN flakes in the grain boundary zones, the growth of ZrB₂ and Zr(C,N) grains was restricted over sintering, resulting in good flexural strength and high fracture toughness [19]. In a study done by Monteverde et al. [20], the addition of 3 vol% HfN assisted the achievement of composites with almost zero percentage of porosity. HfN had a significant contribution to the sintering process as nitrides tend to consume the oxygen content of surface-oxidized phases [20]. Introducing 1 wt% AlN into the ZrB₂-SiC system improved the densification behavior by activating the liquid sintering mechanism, which occurred because of metakaolinite spinel layers [28]. The role of BN additive on the mechanical performance and densification of ZrB₂-SiC revealed that a reaction between BN and ZrO₂ surface oxide could be a reason for the densification improvement and achieving a ~99.8% relative density in the sample with 2.5 vol% BN; however, it is reported that an excessive amount of BN (> 5 vol%) has a destructive influence on the consolidation behavior, deteriorating mechanical properties [29].

To the author's best knowledge, there are a few studies on the influence of Si₃N₄ on the sinterability, densification, mechanical properties, and microstructural evolution in ZrB₂-SiC ceramics [28, 30–32]. As a whole, in all the referenced papers, a nearly fully dense composite and well-densified microstructure compared to the additive-free ZrB₂ ceramic was obtained. Furthermore, fine zirconium diboride grains with interfacial phases, mostly located at triple points, were recorded; however, there is no in-depth investigation using the high-resolution electron transmission microscopy revealing all the phases' characteristics and interfaces of hot-pressed ZrB₂-SiC-Si₃N₄ UHTCs. Therefore, the primary goal of this research is to investigate and detect the probably formed phases in the hot-pressed sample. Besides, hBN

nanosheet formation and their morphology will be discussed. The grain boundary's features, in-situ formed phases, the interface between ZrB₂ and SiC grains, and textural analysis will be explained.

2. Experimental methodology

2.1. Materials and processes

As-received materials used in this work are presented in Table 1. 30 vol% SiC, 4 wt% Resol. 800 (a phenolic resin made in Iran Polymer and Petrochemical Institute) as a binder, 5 wt% Si₃N₄, and the balanced amount of ZrB₂ were balled mixed in the ethanol medium using zirconia cup and balls for 1 h at the speed of 90 rpm. Then, the powder mixture was dried at 90 °C on an HMS 14 rotary evaporator (Tebazma Co., Iran) for 2 h so that the ethanol content was removed, and the agglomerated particles broke down. The dried powder mixture was then passed through a metallic sieve (mesh: 100). Hot-press sintering was conducted in a BN-coated graphite die to avoid any possible reactions between the powder mixture and the carbonaceous die. To pyrolyze the phenolic resin, the samples were heated with a heating rate of 20 °C/min up to 900 °C, and then, the sample was hot-pressed in a vacuum chamber (5×10⁻² Pa) by exerting a pressure of 10 MPa for 2 h at 1900 °C. The ceramic was cooled down after unloading to room temperature with a 5 °C/min cooling rate.

2.2. Characterization

Using the Archimedes method, the bulk density measurement was performed. The relative density was achieved by dividing the measured density by the theoretical one, obtained by the mean of the rule of mixture. The initial powders and sintered sample were phase-analyzed using a Philip PW1800 X-ray diffractometer (XRD) at a current of 30 mA, a voltage of 40 kV, and a wavelength of λ=1.54 Å. The microstructural characterization and chemical analysis of the as-sintered sample were conducted using a FESEM (Mira3 Tescan, Czech Republic) and an energy dispersive spectroscopy (EDS). The TEM sample preparation was carried out via focusing ion beam (FIB) technology, and a Gatan Microscopy Suite (Ametek, USA, ver. 2.11.1404.0.) was utilized to take the HRTEM figures.

3. Results and discussion

According to the SEM images (not shown here) taken from the starting powders used to fabricate the ZrB₂-SiC-Si₃N₄ sample, it is observed that ZrB₂ is in the form of angular particles; however, the SiC and Si₃N₄ powders have irregular morphology. The average ZrB₂, SiC, and Si₃N₄ particle sizes harmonize with the manufacturers' reported values. Although it has been stated in other studies that the surfaces of SiC and ZrB₂ particles are covered with oxide phases such as SiO₂, B₂O₃, and ZrO₂ [33], they could not be detected by XRD because of the low content of such phases.

Table 1. Raw materials data used in this study.

Powder	Average particle size (μm)	Purity (%)
ZrB ₂	2	> 99
α-SiC	5	> 99
Si ₃ N ₄	0.6	> 97

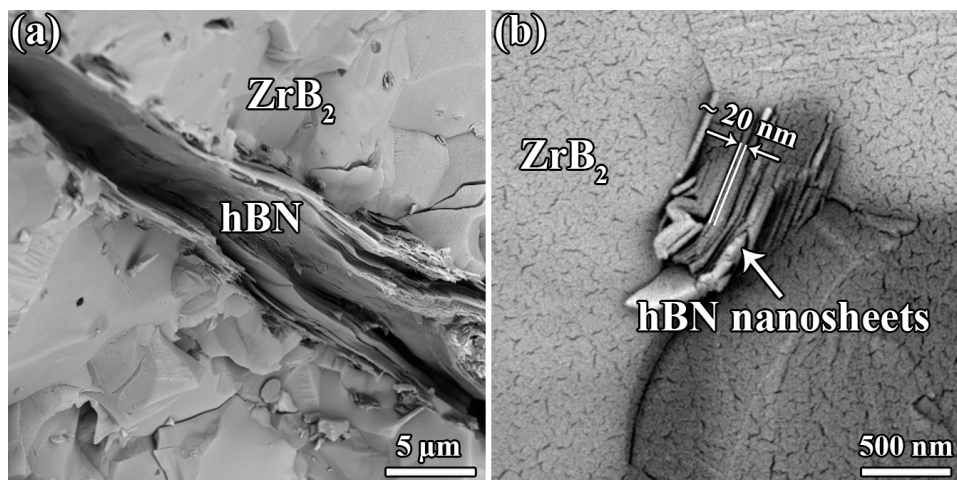
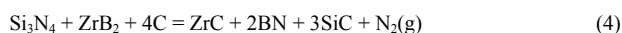


Fig. 1. SEM images of a) the layer-on-layer hBN phase at the ZrB_2 grain boundary and b) the hBN nanosheets' configuration.

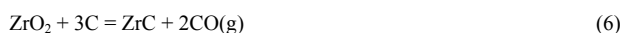
It has been reported that the presence of the SiC phase and the residual C, as a result of phenolic resin decomposition, improves the density of the ZrB_2 ceramics [28]. Moreover, adding Si_3N_4 enhanced the densification during the sintering [34]. It is vital to eliminate the surface oxides from the initial powders, as the mentioned impurities encourage grain coarsening. The residual carbon content can eliminate some surface contaminations, according to Eqs. 1 and 2.



Carbon monoxide can escape out because of the vacuum condition during hot pressing. The oxide phases are reduced to fine ZrB_2 and SiC particles that can assist in achieving a density level close to the theoretical density. Also, the reaction between the Si_3N_4 additive and the B_2O_3 phase (Eq. 3) can lead to the formation of the boron nitride ingredient at the interface of ZrB_2 grains. The morphology, properties, and formation mechanism of boron nitride will be provided later. Depending on the residual amount of Si_3N_4 and C after Eqs. 1–3, two carbide phases, along with boron nitride and N_2 gas, may form based on Eqs. 4 and 5. The formation of the interfacial BN phase prevents ZrB_2 grains from excessive growth.



Therefore, residual carbon and Si_3N_4 additive's role as oxide removers and reducer agents, which causes fine ZrB_2 and SiC formation, led to a relative density of > 99.9% in the as-sintered composite. According to Eq. 6, the synthesis of zirconia carbide is thermodynamically probable. Although carbon monoxide weakens the densification of ZrB_2 -based composites if cannot escape from the sintering composite powders, improved sinterability as a result of the formation of fine interfacial zirconia carbide can be expected. It should be mentioned that, as Eqs. 1–5 possess more negative free Gibbs energy than Eq. 6.



As explained before, the formation of the hBN phase is feasible during hot pressing. The hBN is stable from a thermodynamic point of view at high temperatures [35], so it is expected to observe excellent oxidation resistivity in the as-sintered composite. This phase has a morphology similar to graphite, which consists of hexagonal rings in the basal plane. Each N or B atom only bonds with B or N, respectively. The bonding between B and N atoms is covalent and ionic, but the ionic bonding between layers causes weak inter-planar bonding [36]. The morphology of the hBN in the hot-press sintered ZrB_2 -SiC- Si_3N_4 sample and the configuration of hBN platelets are presented in Fig. 1.

Previously, it was published that the growth mechanism of hBN is identical to graphite, but in a study done by Zhang et al. [37], based on the binary composition feature and lattice symmetry issues in hBN, a novel approach to the growth mechanism of this phase was proposed. They have stated that B and N atoms diffuse at the edges atom-by-atom and this mechanism has a tendency to form two-dimensional hBN in the shapes of triangle or hexagonal. In this study, layer-on-layer formation of hBN in the form of nanosheets including around 15 platelets with an average thickness of ~20 nm was recorded using FESEM.

Utilizing TEM and HRTEM techniques, the microstructure of the hot-pressed composite was deeply characterized. Figs. 4–7 show the ZrB_2 /SiC and ZrB_2 / ZrB_2 interfaces, TEM, HRTEM, and IFFT images from the interior section of a ZrB_2 grain, and the morphology of hBN nanosheets. ZrB_2 is in dark, and SiC is in bright contrasts. Initially, it can be observed that no impurities were identified at the ZrB_2 /SiC interfaces and ZrB_2 / ZrB_2 grain boundaries, which, as discussed before, can be due to the formation of interfacial phases that fill the voids during sintering.

Fig. 2a shows the ZrB_2 /SiC interface's TEM image covered with an amorphous phase between ZrB_2 and SiC. Formation of the SiO_2 phase is thermodynamically probable, according to Eq. 3. Meanwhile, it is a natural surface oxide that forms on the SiC particles. Additionally, based on the melting point temperature of this phase, at the sintering temperature (1900 °C), the presence of this phase in the form of liquid is expected. Another type of ZrB_2 /SiC interface is presented in Fig. 2b.

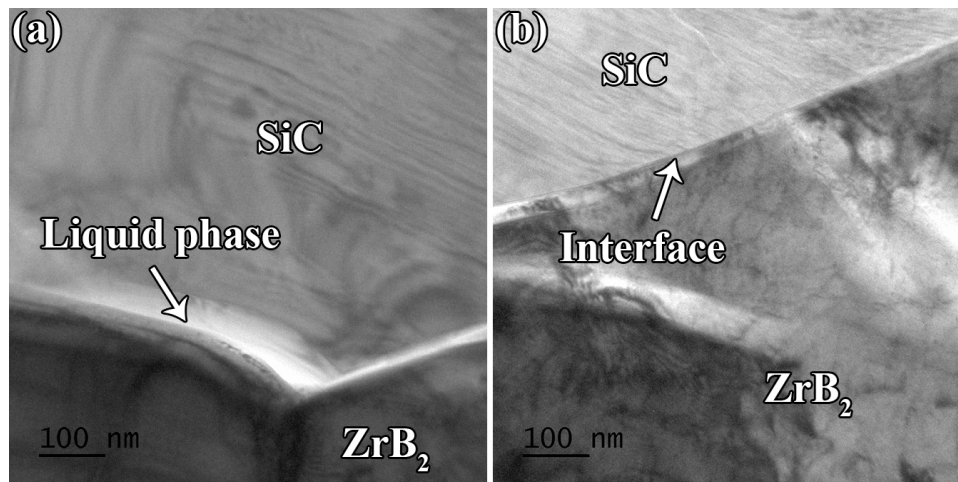


Fig. 2. TEM images of the a) amorphous phase formation along with the ZrB_2/SiC interface and b) clean/smooth ZrB_2/SiC interface.

It is obvious that this interface is clean and smooth, and as these two phases are non-reactive, no sign of chemical interaction was detected. The formation of a clean interface with no distortion proves the fact that ZrB_2 and SiC phases possess the same crystal lattice, as both phases have hexagonal structures. Also, it has been reported that reduction of oxide phases can lead to the development of clean and sharp interfaces [38].

In Fig. 3, the interface of two ZrB_2 neighbors shows a coherent and clean boundary. The most significant feature in this image is the presence of high dislocation density, which can be categorized into i) grain dislocations and ii) grain boundary dislocations. The formation of dislocations within the grains, caused by plastic deformation, has occurred during the hot pressing process. During sintering, exerting pressure aids the densification by compacting the grains, which results in generating dislocations [39]. Furthermore, the dislocation formation can be due to the different thermal expansion coefficients of SiC ($4.3 \times 10^{-6} \text{ K}^{-1}$) and $[\text{40}] \text{ZrB}_2$ ($6.8 \times 10^{-6} \text{ K}^{-1}$) [41]. The dislocation

entanglement within the ZrB_2 grain located on the right side of Fig. 3 is considerable. High-density dislocations can affect mechanical properties through strengthening mechanisms by increased dislocation-induced interactions [42]. Besides, grain boundary dislocations can be formed because of the dislocation propagation resulting from the aforementioned plastic deformation or can be a result of the misorientation between two neighbor grains. Interestingly, most high-temperature dislocations in the interfaces annihilate, which is why the interior area of the ZrB_2 grains contains higher dislocation density [43]. However, some studies investigated the effect of dislocation density increment via work hardening on the mechanical properties improvement, but as ceramics possess covalent or ionic bonding, dislocation strengthening is not considered the main strengthening mechanism [42]. As can be seen, the interface between two ZrB_2 grains is separated by a thin grain boundary. It can be a reason for obtaining high dislocation density grains owing to the lattice mismatch between two ZrB_2 grains.

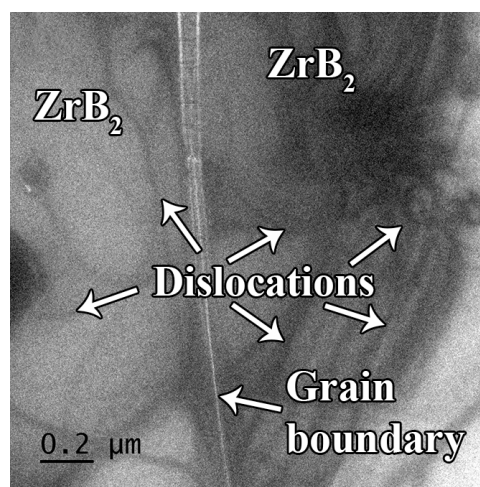


Fig. 3. TEM images of the $\text{ZrB}_2/\text{ZrB}_2$ grain boundary and the network of dislocations within the ZrB_2 grains.

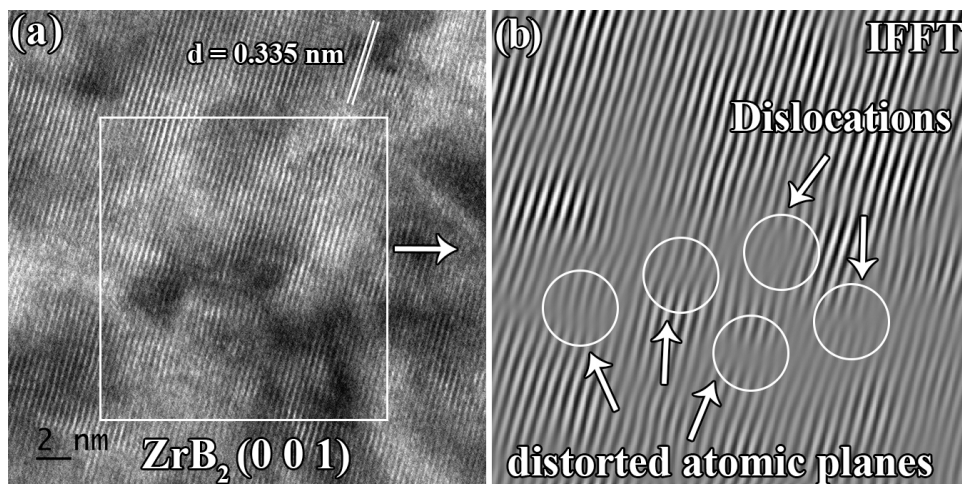


Fig. 4. a) HRTEM image of the interior section of a ZrB_2 grain revealing the d spacing value and indicating the atomic levels of distortion and the formation of edge dislocations and b) IFFT image of the framed section in the left image.

To fully understand the characteristics of the ZrB_2 grains, an HRTEM image from the interior section of a ZrB_2 grain is shown in Fig. 4a. The (001) plane of the ZrB_2 grains with a d-spacing value of 0.335 nm shows that there is an irregular arrangement in the structure, and structural defects can be detected in the crystalline lattice, as a ZrB_2 grain without any structural defects owns a lower d-spacing value (22–27 nm) [40, 41]. Fig. 4b is an IFFT image of the region framed in Fig. 4a. A few distorted atomic planes and two trapped dislocations were detected in such a ZrB_2 grain. These dislocations are edge-type as an extra half-plane of atoms due to applying pressure distorted in the planes of atoms. Also, according to Fig. 3, dislocation lines are parallel or perpendicular to each other (edge dislocations), and there is almost no sign of curved dislocation (screw dislocations). Fig. 3 and Fig. 4b prove that dislocation creep can be one of the main densification mechanisms in this ceramic. Other mechanisms, such as

grain rotation, grain boundary sliding, and plastic yielding, may contribute to densification behavior as well [45]. However, some researchers are questioning the consideration of dislocation creep as a densification mechanism because of restricted slip planes and high Peierls stress [45, 46]. However, a few reports stated high dislocation density in the ceramics sintered under high pressure (100 MPa), and dislocation creep was characterized as the main densification mechanism [46].

hBN nanosheets with a layer-on-layer morphology are exhibited in Fig. 5, a perpendicular view as presented in Fig. 1b. In a study done by Pourmohammadi et al. [29], it is mentioned that the hBN platelets orient perpendicular to the sintering direction, and their formation in the ZrB_2 grain boundaries results in ZrB_2 grain refinement. Moreover, per the Fig. 1 interpretations, the morphology of hBN nanosheets in the form of triangles and hexagonal is observable in Fig. 5.

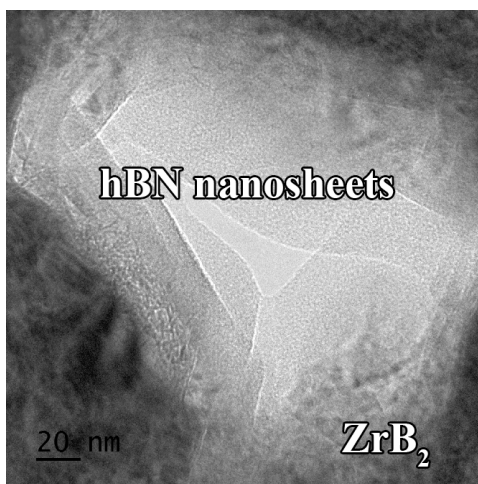


Fig. 5. TEM images of the morphology of hBN nanosheets.

4. Conclusions

The microstructure of as-sintered ZrB₂–SiC UHTC doped with 5 wt% Si₃N₄, manufactured for 2 h under 10 MPa at 1900 °C was characterized using FESEM and HRTEM techniques. The following conclusions were extracted from microscopic observations:

- The FESEM image of the microstructure mainly consisted of ZrB₂ and SiC phases with sharp boundaries that proved the non-reactivity of these phases.
- Electron microscopy observations revealed the formation of layer-on-layer hBN nanosheets consisting of 15 platelets with an average thickness of 20 nm in the shapes of triangle and hexagonal.
- Clean or smooth interfaces and amorphous phase-covered interfaces detected in the ZrB₂/SiC grain boundaries that explained the influence of Si₃N₄ addition and liquid phase formation on the grain boundaries.
- High dislocation density within the ZrB₂ grains, which formed because of the applied pressure during hot pressing, strengthened the fact that dislocation creep can be considered one of the main densification mechanisms.
- The HRTEM image showed a d-spacing of 0.335 nm, which is higher than the d-spacing values of ZrB₂ reported in other studies. Considering the IFFT image, distorted atomic planes and dislocations proved the effect of exerted pressure on the atomic plane's order and dislocation formation.

CRedit authorship contribution statement

Vladimir Bazhin: Conceptualization, Formal Analysis, Methodology, Writing – original draft.

Aleksander Nikolaev: Resources, Supervision, Writing – original draft.

Valeria Esthefania Quiroz Cabascango: Software, Writing – original draft.

Changjin Shao: Supervision.

Genrih Davletov: Validation.

Tatyana Gizatullina: Software.

Vadim Fetisov: Project administration, Writing – review & editing.

Data availability

The data underlying this article will be shared on reasonable request to the corresponding author.

Declaration of competing interest

The authors declare no competing interests.

Funding and acknowledgment

The authors would like to thank the Empress Catherine II Saint Petersburg Mining University.

References

- [1] A. Shima, M. Kazemi, Influence of TiN addition on densification behavior and mechanical properties of ZrB₂ ceramics, *Synth. Sinter.* 3 (2023) 46–53. <https://doi.org/10.53063/synsint.2023.31133>.
- [2] J. Meng, H. Fang, H. Wang, Y. Wu, C. Wei, et al., Effects of refractory metal additives on diboride-based ultra-high temperature ceramics: A review, *Int. J. Appl. Ceram. Technol.* 20 (2023) 1350–1370. <https://doi.org/10.1111/ijac.14336>.
- [3] M. Ghasilzadeh Jarvand, Z. Balak, Oxidation response of ZrB₂–SiC–ZrC composites prepared by spark plasma sintering, *Synth. Sinter.* 2 (2022) 191–197. <https://doi.org/10.53063/synsint.2022.24134>.
- [4] S. Zhu, G. Zhang, Y. Bao, D. Sun, Q. Zhang, et al., Progress in preparation and ablation resistance of ultra-high-temperature ceramics modified C/C composites for extreme environment, *Rev. Adv. Mater. Sci.* 62 (2023) 20220276. <https://doi.org/10.1515/rams-2022-0276>.
- [5] H. Istgaldi, M. Mehrabian, F. Kazemi, B. Nayeji, Reactive spark plasma sintering of ZrB₂–TiC composites: Role of nano-sized carbon black additive, *Synth. Sinter.* 2 (2022) 67–77. <https://doi.org/10.53063/synsint.2022.22107>.
- [6] S. Kim, Y. Oh, L.S. Min, Transmission Electron Microscopy Investigation of Hot-pressed ZrB₂–SiC with B₄C Additive, *J. Korean Ceram. Soc.* 52 (2015) 6–11. <https://doi.org/10.4191/kcers.2015.52.6.462>.
- [7] E. Dodi, Z. Balak, H. Kafashan, Oxidation-affected zone in the sintered ZrB₂–SiC–HfB₂ composites, *Synth. Sinter.* 2 (2022) 31–37. <https://doi.org/10.53063/synsint.2022.21111>.
- [8] F. Monteverde, S. Guicciardi, A. Bellosi, Advances in microstructure and mechanical properties of zirconium diboride based ceramics, *Mater. Sci. Eng. A.* 346 (2003) 310–319. [https://doi.org/10.1016/S0921-5093\(02\)00520-8](https://doi.org/10.1016/S0921-5093(02)00520-8).
- [9] S. Kim, J.-M. Chae, S.-M. Lee, Y.-S. Oh, H.-T. Kim, B.-K. Jang, Change in microstructures and physical properties of ZrB₂–SiC ceramics hot-pressed with a variety of SiC sources, *Ceram. Int.* 40 (2014) 3477–3483. <https://doi.org/10.1016/j.ceramint.2013.09.082>.
- [10] G. Zhang, Z. Deng, N. Kondo, J. Yang, T. Ohji, Reactive Hot Pressing of ZrB₂–SiC Composites, *J. Am. Ceram. Soc.* 32 (2000) 2330–2332. <https://doi.org/10.1111/j.1151-2916.2000.tb01558.x>.
- [11] S.D. Oguntuyi, O.T. Johnson, M.B. Shongwe, Spark plasma sintering of ceramic matrix composite of ZrB₂ and TiB₂: microstructure, densification, and mechanical properties—A review, *Met. Mater. Int.* 27 (2021) 2146–2159. <https://doi.org/10.1007/s12540-020-00874-8>.
- [12] S.C. Zhang, G.E. Hilmas, W.G. Fahrenholtz, Pressureless Sintering of ZrB₂–SiC Ceramics, *Am. Ceram. Soc.* 32 (2008) 26–32. <https://doi.org/10.1111/j.1551-2916.2007.02006.x>.
- [13] R. Zhang, R. He, X. Zhang, D. Fang, Microstructure and mechanical properties of ZrB₂–SiC composites prepared by gelcasting and pressureless sintering, *Int. J. Refract. Met. Hard Mater.* 43 (2014) 83–88. <https://doi.org/10.1016/j.ijrmhm.2013.11.008>.
- [14] D. Sciti, L. Silvestroni, V. Medri, S. Guicciardi, Pressureless sintered in situ toughened ZrB₂–SiC platelets ceramics, *J. Eur. Ceram. Soc.* 31 (2011) 2145–2153. <https://doi.org/10.1016/j.jeurceramsoc.2011.04.040>.
- [15] X. Wang, W. Guo, G. Zhang, Pressureless sintering mechanism and microstructure of ZrB₂–SiC ceramics doped with boron, *Scr. Mater.* 61 (2009) 177–180. <https://doi.org/10.1016/j.scriptamat.2009.03.030>.
- [16] R. Inoue, Y. Arai, Y. Kubota, Y. Kogo, K. Goto, Initial oxidation behaviors of ZrB₂–SiC–ZrC ternary composites above 2000 °C, *J. Alloys Compd.* 731 (2018) 310–317. <https://doi.org/10.1016/j.jallcom.2017.10.034>.
- [17] C. Ojalvo, F. Guiberteau, A.L. Ortiz, Fabricating toughened super-hard B₄C composites at lower temperature by transient liquid-phase assisted spark plasma sintering with MoSi₂ additives, *J. Eur. Ceram. Soc.* 39 (2019) 2862–2873. <https://doi.org/10.1016/j.jeurceramsoc.2019.03.035>.
- [18] J. Zou, G.J. Zhang, G.J. Hu, T. Nishimura, Y. Sakka, et al., Strong ZrB₂–SiC–WC Ceramics at 1600 °C, *J. Am. Ceram. Soc.* 878 (2012) 874–878. <https://doi.org/10.1111/j.1551-2916.2011.05062.x>.

- [19] W. Wu, G. Zhang, Y. Kan, Y. Sakka, Synthesis, microstructure and mechanical properties of reactively sintered ZrB₂-SiC-ZrN composites, *Ceram. Int.* 39 (2013) 7273–7277. <https://doi.org/10.1016/j.ceramint.2013.02.028>.
- [20] F. Monteverde, A. Bellosi, Efficacy of HfN as sintering aid in the manufacture of ultrahigh-temperature metal diborides-matrix ceramics, *J. Mater. Res.* 19 (2004) 3576–3585. <https://doi.org/10.1557/JMR.2004.0460>.
- [21] Y. Yang, M. Li, L. Xu, J. Xu, Y. Qian, et al., Oxidation behaviours of ZrB₂-SiC-MoSi₂ composites at 1800 °C in air with different pressures, *Corros. Sci.* 157 (2019) 87–97. <https://doi.org/10.1016/j.corsci.2019.05.027>.
- [22] L. Silvestroni, D. Sciti, Densification of ZrB₂-TaSi₂ and HfB₂-TaSi₂ Ultra-High-Temperature Ceramic Composites, *Am. Ceram. Soc.* 1930 (2011) 1920–1930. <https://doi.org/10.1111/j.1551-2916.2010.04317.x>.
- [23] O.N. Grigoriev, B.A. Galanov, V.A. Lavrenko, A.D. Panasyuk, S.M. Ivanov, et al., Oxidation of ZrB₂-SiC-ZrSi₂ ceramics in oxygen, *J. Eur. Ceram. Soc.* 30 (2010) 2397–2405. <https://doi.org/10.1016/j.jeurceramsoc.2010.03.016>.
- [24] X. Zhang, W. Li, C. Hong, W. Han, J. Han, A novel development of ZrB₂/ZrO₂ functionally graded ceramics for ultrahigh-temperature application, *Scr. Mater.* 59 (2008) 1214–1217. <https://doi.org/10.1016/j.scriptamat.2008.08.014>.
- [25] X. Zhang, X. Li, J. Han, W. Han, C. Hong, Effects of Y₂O₃ on microstructure and mechanical properties of ZrB₂-SiC ceramics, *J. Alloys Compd.* 465 (2008) 506–511. <https://doi.org/10.1016/j.jallcom.2007.10.137>.
- [26] M. Shahedi, B. Nayebi, M. Ghassemi, M. Shokouhimehr, Investigation of hot pressed ZrB₂-SiC-carbon black nanocomposite by scanning and transmission electron microscopy, *Ceram. Int.* 45 (2019) 16759–16764. <https://doi.org/10.1016/j.ceramint.2019.05.211>.
- [27] F. Yang, X. Zhang, J. Han, S. Du, Mechanical properties of short carbon fiber reinforced ZrB₂-SiC ceramic matrix composites, *Mater. Lett.* 62 (2008) 2925–2927. <https://doi.org/10.1016/j.matlet.2008.01.076>.
- [28] Z. Ahmadi, B. Nayebi, M. Shahedi Asl, M. Ghassemi Kakroudi, Fractographical characterization of hot pressed and pressureless sintered AlN-doped ZrB₂-SiC composites, *Mater. Charact.* 110 (2015) 77–85. <https://doi.org/10.1016/j.matchar.2015.10.016>.
- [29] N. Pourmohammadi, M. Ghassemi, M. Shahedi, Role of h-BN content on microstructure and mechanical properties of hot-pressed ZrB₂-SiC composites, *Ceram. Int.* 46 (2020) 21533–21541. <https://doi.org/10.1016/j.ceramint.2020.05.255>.
- [30] S.K. Thimmappa, B.R. Golla, V.V.B. Prasad, B. Majumdar, B. Basu, Phase stability, hardness and oxidation behaviour of spark plasma sintered, *Ceram. Int.* 45 (2019) 9061–9073. <https://doi.org/10.1016/j.ceramint.2019.01.243>.
- [31] M. Mallik, K.K. Ray, R. Mitra, Effect of Si₃N₄ Addition on Compressive Creep Behavior of Hot-Pressed ZrB₂-SiC Composites, *J. Am. Ceram. Soc.* 2964 (2014) 2957–2964. <https://doi.org/10.1111/jace.13022>.
- [32] Z. Bahararjmand, M.A. Khalilzadeh, F. Saberi-Movahed, T.H. Lee, J. Wang, et al., Role of Si₃N₄ on microstructure and hardness of hot-pressed ZrB₂-SiC composites, *Synth. Sinter.* 1 (2021) 34–40. <https://doi.org/10.53063/synsint.2021.1113>.
- [33] M.D. Alviri, M.G. Kakroudi, B. Salahimehr, R. Alaghmandfard, M.S. Asl, M. Mohammadi, Microstructure, mechanical properties, and oxidation behavior of hot-pressed ZrB₂-SiC-B₄C composites, *Ceram. Int.* 47 (2020) 9627–9634. <https://doi.org/10.1016/j.ceramint.2020.12.101>.
- [34] Z. Ahmadi, B. Nayebi, M. Shahedi Asl, M. Ghassemi Kakroudi, I. Farahbakhsh, Sintering behavior of ZrB₂-SiC composites doped with Si₃N₄: a fractographical approach, *Ceram. Int.* 43 (2017) 9699–9708. <https://doi.org/10.1016/j.ceramint.2017.04.144>.
- [35] T.T. Yoichi Kubota, K. Watanabe, Osamu Tsuda, Deep Ultraviolet Light-Emitting Hexagonal Boron Nitride Synthesized at Atmospheric Pressure, *Science.* 317 (2007) 932–935. <https://doi.org/10.1126/science.1144216>.
- [36] N. Ooi, V. Rajan, J. Gottlieb, Y. Catherine, J.B. Adams, Structural properties of hexagonal boron nitride, *Model. Simul. Mater. Sci. Eng.* 14 (2006) 515–535. <https://doi.org/10.1088/0965-0393/14/3/012>.
- [37] Z. Zhang, Y. Liu, Y. Yang, B.I. Yakobson, Growth Mechanism and Morphology of Hexagonal Boron Nitride, *Nano Lett.* 16 (2016) 1398–1403. <https://doi.org/10.1021/acs.nanolett.5b04874>.
- [38] C. Xia, S.A. Delbari, Z. Ahmadi, M. Shahedi Asl, M. Ghassemi Kakroudi, et al., Electron microscopy study of ZrB₂-SiC-AlN composites: Hot-pressing vs. pressureless sintering, *Ceram. Int.* 46 (2020) 29334–29338. <https://doi.org/10.1016/j.ceramint.2020.08.054>.
- [39] C. Hu, Y. Sakka, J. Gao, H. Tanaka, S. Grasso, Microstructure characterization of ZrB₂-SiC composite fabricated by spark plasma sintering with TaSi₂ additive, *J. Eur. Ceram. Soc.* 32 (2012) 1441–1446. <https://doi.org/10.1016/j.jeurceramsoc.2011.08.024>.
- [40] R.C. Li, Z. Bradt, Thermal Expansion of the Hexagonal (6H) Polytype of Silicon Carbide, *J. Am. Ceram. Soc.* 66 (1986) 863–866. <https://doi.org/10.1111/j.1151-2916.1986.tb07385.x>.
- [41] N.L. Okamoto, M. Kusakari, K. Tanaka, H. Inui, M. Yamaguchi, S. Otani, Temperature dependence of thermal expansion and elastic constants of single crystals of ZrB₂ and the suitability of ZrB₂ as a substrate for GaN film, *J. Appl. Phys.* 93 (2003) 88–93. <https://doi.org/10.1063/1.1525404>.
- [42] H. Ma, J. Zou, J. Zhu, L. Liu, G. Zhang, Segregation of tungsten atoms at ZrB₂ grain boundaries in strong ZrB₂-SiC-WC ceramics, *Scr. Mater.* 157 (2018) 76–80. <https://doi.org/10.1016/j.scriptamat.2018.07.038>.
- [43] J. Liang, Y. Wang, S. Meng, Interface and defect characterization in hot-pressed ZrB₂-SiC ceramics, *Int. J. Refract. Met. Hard Mater.* 29 (2011) 341–343. <https://doi.org/10.1016/j.ijrmhm.2010.12.010>.
- [44] Z. Liu, Y. Gong, W. Zhou, L. Ma, J. Yu, et al., Ultrathin high-temperature oxidation-resistant coatings of hexagonal boron nitride, *Nat. Commun.* 4 (2013) 1–8. <https://doi.org/10.1038/ncomms3541>.
- [45] J. Gu, J. Zou, J. Liu, H. Wang, J. Zhang, et al., Sintering highly dense ultra-high temperature ceramics with suppressed grain growth, *J. Eur. Ceram. Soc.* 40 (2020) 1086–1092. <https://doi.org/10.1016/j.jeurceramsoc.2019.11.056>.
- [46] M. Gendre, A. Maître, G. Trolliard, A study of the densification mechanisms during spark plasma sintering of zirconium (oxy-) carbide powders, *Acta Mater.* 58 (2010) 2598–2609. <https://doi.org/10.1016/j.actamat.2009.12.046>.